Journal of Magnetic Resonance **156,** 282–294 (2002)
doi:10.1006/jmre.2002.2565

Optimizing Delays in the MBOB, Broadband HMBC, and Broadband XLOC NMR Pulse Sequences

Thomas Schulte-Herbrüggen,* Axel Meissner,* Alexandra Papanikos,† Morten Meldal,† and Ole Winneche Sørensen*,[1]

*Department of Chemistry, †Center for Solid-Phase Organic Combinatorial Chemistry (SPOCC), Carlsberg Laboratory, Gamle Carlsberg Vej 10, DK-2500 Valby, Denmark

Received February 6, 2002; revised May 7, 2002; published online July 3, 2002

The MBOB, broadband HMBC, and broadband XLOC NMR pulse sequences (A. Meissner and O. W. Sørensen (2000, *Magn. Reson. Chem.* 38, 981–984; 2001, 39, 49–52)) were introduced as a means of obtaining heteronuclear long-range correlation spectra with broadband excitation over an interval of heteronuclear long-range *J* coupling constants. However, it is not trivial what combination of delays to choose for a given purpose, particularly if one-bond and long-range correlation spectra are obtained simultaneously as in MBOB. This paper presents a way to determine sets of delays for MBOB, broadband HMBC, and broadband XLOC resolving the problem. The results tabulated suit various ranges of *J* coupling constants and transverse relaxation times. © 2002 Elsevier Science (USA)

Key Words: **MBOB; HMBC; broadband HMBC; broadband XLOC; HR-MAS.**

INTRODUCTION

Techniques providing correlations via heteronuclear long-range *J* coupling constants are indispensable for NMR structure determination of small molecules. The field was boosted by the advent of high-quality pulsed field gradients that yield excellent artifact suppression. All methods of choice involve proton detection, and many variations based on the HMBC scheme (*1*) have been suggested.

The HMBC technique includes an excitation delay Δ to build up antiphase magnetization via the heteronuclear long-range coupling constants prior to excitation of heteronuclear zero- and double-quantum coherence evolving in the evolution period of the two-dimensional experiment. The excitation efficiency is proportional to $\sin(\pi J \Delta)$, and this function cannot be optimized for all J's in a single experiment. Thus broadband excitation is a problem in the HMBC technique. A widely used solution is to select a Δ slightly smaller than the inverse of the expected largest relevant J coupling constant in the sample, which typically is $\Delta = 65$ ms in ^{13}C–^{1}H long-range correlations. However, this is not efficient for the smallest J's that call for longer delays Δ. On the other hand, longer delays run the risk that $\sin(\pi J \Delta)$ might vanish for some of the larger J coupling constants. The broadband HMBC (*2*), broadband XLOC (*3–6*), and MBOB (*2*) solution to the nonuniform excitation problem is to combine spectra recorded with different delays Δ in absolute-value mode. Alternative solutions to the problem of nonuniform excitation include accordion-type incrementation of the Δ delay along with t_1. However, the uniformity of this approach comes at a penalty of additional multiplet structure in the indirect dimension, which is undesirable for two reasons: (i) lowered sensitivity because the intensity is spread out on more multiplet components, (ii) potential spectral ambiguities caused by overlap of the extended multiplets.

This paper describes in detail how to determine suitable sets of Δ values for various ranges of heteronuclear J coupling constants. The MBOB (*2*), the broadband HMBC, and the broadband XLOC (*2, 6*) sequences are outlined in Fig. 1; the latter two explicitly include a third-order low-pass J filter.

THEORY

In a heteronuclear two-spin subsystem the build-up of antiphase magnetization for coherence transfer during a delay Δ is determined by the amplitude function

$$f(\Delta, J, T_2) = \sin(\pi J \Delta)\, e^{-\Delta/T_2}, \qquad [1]$$

which has its maximum at

$$\Delta_m(J, T_2) = \frac{1}{\pi J} \arctan(\pi J T_2)$$
$$= \Delta_m(J, L) = \frac{1}{\pi J} \arctan(J/L). \qquad [2]$$

Here $L = 1/(\pi T_2)$ is the Lorentzian linewidth in Hertz associated with an averaged relaxation time T_2. The function $\Delta_m(J, L)$ is outlined in Fig. 2a. Clearly, the sine function in Eq. [1] has a dominating influence on the product for small linewidths while the damping by the exponential function grows with increasing linewidth to the extent that the maxima in Eq. [2] become rather insensitive to J for large linewidth. Hence a single Δ delay is adequate in that limit, whereas Δ_m is strongly dependent on

[1] To whom correspondence should be addressed. E-mail: ows@crc.dk.

1090-7807/02 $35.00

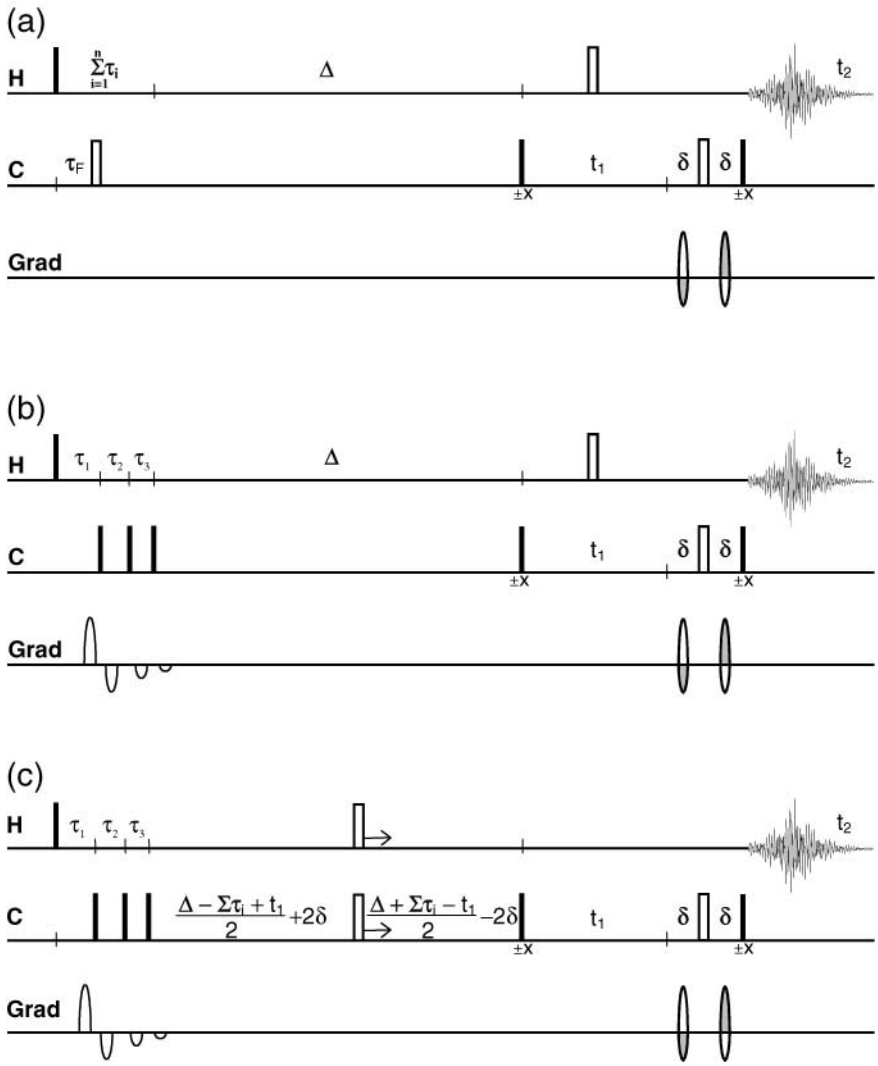

FIG. 1. Pulse sequences for MBOB, broadband HMBC, and broadband XLOC. Filled and open bars represent $\pi/2$ and π pulses, respectively. Pulsed field gradients are indicated as bell shapes. Pulse phases with the prefix $\pm$ indicate independent two-step phase cycles with alternating receiver phase. Δ represents four different delays according to the broadband excitation scheme to generate subspectra for combination in absolute value, while δ is the gradient delay. Recommended individual delays for the low-pass J filter are $\tau_1 = (J^{\max} + J^{\min})^{-1}$ for the first-order filter, $\{\tau_1 = 1/2[J^{\min} + 0.146(J^{\max} - J^{\min})]^{-1}; \tau_2 = 1/2[J^{\max} - 0.146(J^{\max} - J^{\min})]^{-1}\}$ for the second-order filter, and $\{\tau_1 = 1/2[J^{\min} + 0.07(J^{\max} - J^{\min})]^{-1}; \tau_2 = (J^{\max} + J^{\min})^{-1}; \tau_3 = 1/2[J^{\max} - 0.07(J^{\max} - J^{\min})]^{-1}\}$ for the third-order filter where the expected range to cover is $J^{\min} < {}^1J_{\mathrm{CH}} < J^{\max}$. The ratio of the heteronuclear gradient echo gradients after t_1 is $+5:-3$ for echo selection and $-3:+5$ for antiecho selection, respectively. The ratio for the low-pass J filter gradients in (b) and (c) is in both cases $+3.5:-2:-1:-0.5$. (a) MBOB pulse sequence for simultaneous observation of one-bond and long-range correlations. For the low-pass J filter the delay τ_F is cycled through 2^n steps for an nth order filter, i.e., $\{0, \tau_1\}$, $\{0, \tau_1, \tau_2, \tau_1 + \tau_2\}$, $\{0, \tau_1, \tau_2, \tau_3, \tau_1 + \tau_2, \tau_1 + \tau_3, \tau_2 + \tau_3, \tau_1 + \tau_2 + \tau_3\}$ for a first, second, and third order filter, respectively. Two data sets are recorded for each Δ delay with $\tau_F = \{0, \tau_1 + \tau_2, \tau_1 + \tau_3, \tau_2 + \tau_3\}$ (*even*), and $\tau_F = \{\tau_1, \tau_2, \tau_3, \tau_1 + \tau_2 + \tau_3, \}$ (*odd*), respectively. The linear combinations (*even* + *odd*) and (*even* − *odd*) of the data sets yield the long-range and one-bond correlation MBOB spectra, respectively. (b) Broadband HMBC pulse sequence with a third-order low-pass J filter. (c) Broadband XLOC pulse sequence with a third-order low-pass J filter.

J for small molecules with relatively long T_2 relaxation times; here MBOB copes with the variation in Δ_m. There is as a rule of thumb a call for MBOB whenever $\Delta_m({}^nJ_{\min}, L) > 1/{}^nJ_{\max}$ where ${}^nJ_{\min}$ and ${}^nJ_{\max}$ are the smallest and largest expected long-range J coupling constants of interest in the molecule under investigation.

Inserting Eq. [2] into Eq. [1] and exploiting the identity $\sin(\arctan(x)) = 1/\sqrt{1+x^2}$ yields the following maximum amplitude as a function of the J coupling constant and the linewidth

$$f_m(J, L) = \frac{J}{L} \cdot \frac{1}{\sqrt{1 + (J/L)^2}}\, e^{-\frac{\arctan(J/L)}{J/L}}. \qquad [3]$$

Moreover, the actual signal intensity is affected by the partial cancellation caused by overlap of the two components in

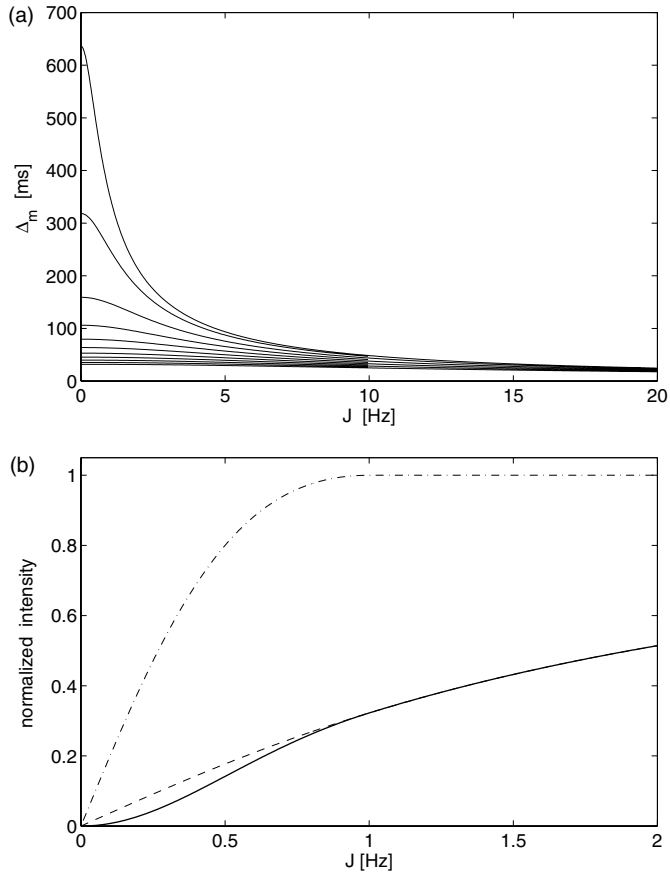

FIG. 2. (a) Delays Δ_m ensuring maximum coherence transfer amplitude via a given individual J coupling constant (see Eq. [2]). The traces correspond to Lorentzian linewidths of 0.5, 1, 2, 3, . . . , 10 Hz, respectively. At small linewidths, the optimal setting greatly depends on J, while in large molecules it is nearly independent of the coupling constant. For clarity, every second trace is terminated at 10 Hz. (b) Maximum amplitudes for the build-up of antiphase magnetization $2I_xS_z$ as a function of the coupling constant J_{IS}. The delay for coherence transfer is set as Δ_m as in (a) and Eq. [2] with a Lorentzian linewidth of 1 Hz. Dashed line (- -), maximum transfer function f_m according to Eq. [3]; dash-dotted line (−·), normalized maximal antiphase signal intensity s_m in magnitude mode as in Eq. [7]; solid line (−), effective maximal signal $g_m = s_m \cdot f_m$ defined by Eq. [8].

the Lorentzian antiphase doublet $S(\nu)$. Assuming that the two components in the antiphase doublet have the same linewidth, the signal takes the form of a difference of two complex Lorentzians

$$S(\nu) = \frac{1}{\pi}\left\{\frac{1}{L - i(2\nu - J)} - \frac{1}{L - i(2\nu + J)}\right\}. \qquad [4]$$

When discussing the two-dimensional (2D) long-range correlation spectra, it is sufficient to consider the 1D signal function $S(\nu)$, because standard data processing discards the dispersive component after Fourier transformation in the indirect dimension. The final spectra are presented in magnitude mode; so the spectral function to analyze is the absolute value $|S(\nu)|$. The frequencies at the critical points of $|S(\nu)|$ are

$$\nu_0 = 0 \qquad \text{and} \qquad \nu_\pm = \pm\frac{1}{2}\sqrt{J^2 - L^2}. \qquad [5]$$

As long as $|J| > L$, $|S(\nu_0)|$ is a relative minimum and the $|S(\nu_\pm)|$ are the two absolute maxima. However, at small coupling constants $|J| \le L$, the two maxima coalesce to a single one at $|S(\nu_0)|$. Thus the maximum signal may be expressed as a function of the coupling constant J and the linewidth L as

$$S_m(J, L) = \max|S(\nu)| = \begin{cases} \frac{2}{\pi}\frac{J}{J^2+L^2} & \text{for } |J| \le L \\ \frac{1}{\pi}\frac{1}{L} & \text{for } |J| > L. \end{cases} \qquad [6]$$

Note that for $|J| > L$ the maxima are independent of the coupling constant and coincide with the amplitude of the real part of a single Lorentzian. Hence it is useful to define a normalized signal magnitude according to

$$s_m(J, L) = \frac{S_m(J, L)}{(\pi\, L)^{-1}}. \qquad [7]$$

To sum up, this scaling by partial overlap in a doublet can be combined with the previous results of Eq. [3] for optimum coherence transfer to take the final form

$$g_m(J, L) = s_m(J, L) \cdot f_m(J, L) = \begin{cases} \frac{2(J/L)^2}{[1+(J/L)^2]^{3/2}}\, e^{-\frac{\arctan(J/L)}{J/L}} & \text{for } |J|/L \le 1 \\ \frac{(J/L)}{[1+(J/L)^2]^{1/2}}\, e^{-\frac{\arctan(J/L)}{J/L}} & \text{for } |J|/L > 1, \end{cases} \qquad [8]$$

illustrated in Fig. 2b. Given a Lorentzian linewidth L, it denotes the maximum coherence transfer signal magnitude in an antiphase doublet separated by the coupling constant J. These optima can only be obtained by setting the delay $\Delta = \Delta_m(J, L)$ individually according to Fig. 2a and Eq. [2]. Obviously, this is neither possible for all J nor for all T_2 values simultaneously. With the linewidth as a parameter, the goal of this work is to approximate the optima of Eq. [8] over a wide range of pertinent J coupling constants by combining several experiments taken with different Δ_i. Figure 2a clearly indicates that these combinations are particularly advantageous for narrow lines, i.e., in small molecules. Moreover, the combination can be chosen such as to provide the long-range correlation information in the HMBC part, and the one-bond correlations in a separate spectrum

obtained by a different combination of the same experimental data sets. In order to separate the two domains of coupling constants, nondestructive low- and high-pass J filters are necessary.

In principle, the optimization considerations outlined here are also valid for larger spin systems comprising additional protons. In practice, however, unresolved ^{1}H–^{1}H proton coupling constants attenuate the signals even further in the sense of a smaller effective T_2 (*vide infra*). This problem inherent in HMBC spectra can partly be resolved by using selective refocusing pulses (*7*) and the benefits of MBOB are independent of the selectivity of the ^{1}H refocusing pulses.

J FILTERS

The oscillations due to the one-bond J's in $\sin(\pi J\Delta)$ are fast compared to those of the long-range J's, so slight changes in Δ values will have little effect for the long-range J's, but they can have a dramatic impact on the intensities in the one-bond correlation spectrum. Furthermore, the nondestructive J filter acting as a low-pass J filter in the MBOB long-range correlation spectrum does not significantly scale the long-range J's, but it does affect the intensities in the MBOB one-bond correlation spectrum, particularly when large one-bond J ranges must be covered.

The recommended individual J filter delays τ_i are independent of Δ. For a second-order filter they are (*9*) $\{\tau_1 = 1/2[J^{\min} + 0.146(J^{\max} - J^{\min})]^{-1}; \tau_2 = 1/2[J^{\max} - 0.146(J^{\max} - J^{\min})]^{-1}\}$ while in a third-order J filter they read (*10*) $\{\tau_1 = 1/2[J^{\min} + 0.07(J^{\max} - J^{\min})]^{-1}; \tau_2 = (J^{\max} + J^{\min})^{-1}; \tau_3 = 1/2[J^{\max} - 0.07(J^{\max} - J^{\min})]^{-1}\}$. Both cases cover an expected range $J^{\min} < {}^1J_{CH} < J^{\max}$. The data set with $\tau_F = \{0, \tau_1+\tau_2, \tau_1+\tau_3, \tau_2+\tau_3\}$ is referred to as *even*, while $\tau_F = \{\tau_1, \tau_2, \tau_3, \tau_1+\tau_2+\tau_3,\}$ denotes the *odd* counterpart. *Even* and *odd* data sets are combined as described in the caption to Fig. 1 and in Ref. (*2*). Thereafter linear combinations in absolute-value mode are taken over the Δcycle, i.e., $\sum_{\Delta_i} |F^{\text{Even+Odd}}|$ for the long-range spectrum and $\sum_{\Delta_i} |F^{\text{Even-Odd}}|$ for the one-bond MBOB spectrum (*2, 8*).

The intensity functions for the MBOB one-bond spectrum are (*2*)

$$F^{\text{Even-Odd}} = \sin(\pi J\Delta) \prod_{i=1}^{2} \sin(\pi J\tau_i) \cdot \exp\left\{-\frac{1}{T_2}\left(\Delta + \sum_{i=1}^{n} \tau_i\right)\right\}$$

for a second-order J filter [9a]

$$F^{\text{Even-Odd}} = \cos(\pi J\Delta) \prod_{i=1}^{3} \sin(\pi J\tau_i) \cdot \exp\left\{-\frac{1}{T_2}\left(\Delta + \sum_{i=1}^{n} \tau_i\right)\right\}$$

for a third-order J filter [9b]

and for the long-range MBOB spectrum (*3*)

$$F^{\text{Even+Odd}} = \sin(\pi J\Delta) \prod_{i=1}^{n} \cos(\pi J\tau_i) \cdot \exp\left\{-\frac{1}{T_2}\left(\Delta + \sum_{i=1}^{n} \tau_i\right)\right\}, \qquad n = 2, 3, \quad [10]$$

where n is the order of the J filter.

OPTIMIZATION PROCEDURES

For the individual linewidths of 0.5, 1, 2, and 3 Hz, least-squares fits are used to search for suitable sets of N different Δ values $\{\Delta_1, \Delta_2, \ldots, \Delta_N\}$. In order to counterbalance the inevitable intensity loss by partial cancellation within antiphase doublets separated by small J's, the amplitude target function in the long-range J coupling constant domain puts particular weight on the small long-range coupling constants thus deliberately exceeding the amplitudes actually achievable (see Eq. [8]). It starts with the weight w in the limit ${}^nJ = 0$ and decays quadratically up to an amplitude N at the largest long-range coupling of interest ${}^nJ = {}^nJ^{\max}$ according to

$$t({}^nJ) = \frac{w - N}{({}^nJ^{\max})^2}({}^nJ - {}^nJ^{\max})^2 + N \qquad \text{with } {}^nJ \in [0; {}^nJ^{\max}]. \quad [11]$$

For the one-bond J domain, however, the target function is constant

$$t({}^1J) = N \qquad \text{with } {}^1J \in [120 \text{ Hz}; 225 \text{ Hz}]. \quad [12]$$

Using independent combinations of the weighting parameters $w \in \{20, 50, 100\}$ and, according to the class of substances (*vide infra*), ${}^nJ^{\max} \in \{4, 8, 16, 25, 50 \text{ Hz}\}$ for each of the linewidths of 0.5, 1, 2, 3 Hz, an array of least-squares fits was performed starting from a multitude of initial conditions. $N = 4$ was chosen as a compromise between broadband excitation and size of the Δ cycle. ($N = 5$ did not provide an advantage significant enough to justify the longer measurement times, whereas $N = 3$ in turn entailed dips in the broadband ranges of couplings studied here. In cases of narrower intervals of coupling constants of interest, $N = 3$ may suffice, which however is not the typical situation when recording spectra of unknown substances.) More than 7000 initial delays were used to cover the range from 50 to 500 ms in steps of 25 ms for each initial set ($\Delta_1^0 \geq \Delta_2^0 \geq \Delta_3^0 \geq \Delta_4^0$). The results obtained by the least-squares fit correspond to different minima, which can be exploited to put emphasis on different windows of long-range couplings of interest. For instance, the ^{13}C–^{1}H coupling constants ${}^2J_{CH}$ fall below 8 Hz in aliphatic ketones, 16 Hz in

TABLE 1

Delay Sets and Performance Characteristics for *Ultra* and Broadband MBOB Optimized for a Lorentzian Linewidth of 0.5 Hz

No.	Δ_1 [ms]	Δ_2 [ms]	Δ_3 [ms]	Δ_4 [ms]	[$^nJ_{90\%}$]	[$^nJ_{75\%}$]	[$^nJ_{50\%}$]	[$^nJ_{25\%}$]	a_{90}	a_{75}	a_{50}	a_{25}	^nJ(max)	$^na_{\max}$	^nJ(min)	$^na_{\min}$	^na	^1J(max)	$^1a_{\max}$	^1J(max)	$^1a_{\min}$	^1a
1	*501.5*	*432.8*	*397.9*	*323.5*	0.03 1.20	0.03 1.50	0.03 1.83	0.03 9.20	0.32	0.35	0.36	0.33	1.20	0.50	27.73	0.05	0.29	145.55	0.42	202.32	0.04	0.23
2	170.6	168.6	167.4	165.4	1.63 3.57	1.00 4.13	0.03 4.83	0.03 5.40	0.71	0.66	0.54	0.52	2.97	0.76	5.93	0.02	0.43	162.21	0.43	220.66	0.16	0.33
3	213.7	174.1	104.1	90.4	— —	1.43 4.07	0.27 8.70	0.03 49.97	—	0.62	0.55	0.45	3.13	0.68	46.80	0.22	0.45	154.58	0.64	215.69	0.10	0.35
4	192.2	139.2	107.9	105.1	2.43 3.83	1.50 4.80	0.40 7.77	0.03 36.10	0.72	0.67	0.55	0.48	3.50	0.74	36.43	0.16	0.45	150.73	0.59	225.00	0.15	0.35
5	112.6	97.3	73.0	64.2	3.97 6.40	2.67 7.70	1.27 10.10	0.03 49.97	0.79	0.74	0.63	0.49	5.50	0.81	41.10	0.31	0.49	152.55	0.62	210.65	0.11	0.39
6	98.7	89.8	72.5	63.8	4.13 7.20	2.87 8.47	1.40 9.93	0.03 49.97	0.81	0.76	0.67	0.49	5.97	0.83	30.40	0.29	0.49	153.81	0.62	217.16	0.16	0.39
7	95.7	79.9	63.6	55.0	4.73 7.67	3.23 9.17	1.63 12.17	0.03 49.97	0.81	0.76	0.65	0.50	6.50	0.83	49.97	0.29	0.50	125.81	0.62	225.00	0.14	0.39
8	106.5	89.9	58.4	55.4	4.80 6.57	3.13 8.30	1.53 16.27	0.03 49.97	0.78	0.73	0.62	0.50	6.00	0.79	18.77	0.26	0.50	167.81	0.59	225.00	0.19	0.39
9	101.0	72.5	63.8	39.4	— —	3.63 9.00	1.80 26.10	0.03 49.97	—	0.73	0.59	0.50	6.57	0.78	49.50	0.24	0.50	177.33	0.59	212.89	0.08	0.40
10	88.6	67.7	58.8	41.4	5.80 8.17	3.87 10.17	2.00 22.33	0.17 49.97	0.80	0.75	0.59	0.50	7.27	0.81	45.13	0.24	0.50	148.00	0.64	212.61	0.21	0.40
11	55.1	46.7	36.7	32.7	8.40 13.43	5.97 15.97	3.30 20.80	1.07 49.97	0.84	0.79	0.68	0.54	11.07	0.86	21.40	0.43	0.53	128.75	0.58	225.00	0.11	0.41
12	54.8	46.0	36.8	33.0	8.40 13.57	5.97 16.07	3.33 20.90	1.10 49.97	0.85	0.80	0.68	0.54	11.13	0.86	27.17	0.42	0.53	129.45	0.57	225.00	0.13	0.41
13	56.6	48.4	36.3	32.5	8.37 12.97	5.90 15.57	3.27 30.53	1.07 49.97	0.84	0.79	0.60	0.54	10.83	0.85	35.33	0.39	0.53	161.16	0.65	220.87	0.21	0.41
	65	65	65	65	5.07 9.63	3.63 11.03	1.93 12.70	0.03 14.07	0.85	0.80	0.71	0.60	7.63	0.88	30.77	0.00	0.49	153.88	0.74	192.31	0.00	0.40
	100	100	100	100	3.13 6.17	2.17 7.10	0.97 8.20	0.03 9.13	0.80	0.75	0.66	0.57	5.00	0.84	10.00	0.00	0.48	159.97	0.70	225.00	0.00	0.37

Note. Δ_i, delays in ms; [$^nJ_{x\%}$], left-most intervals in which at least $x\%$ of the maximal transfer amplitude is actually achieved; a_x, mean in the respective interval; $^{n/1}J$(max/min), long-range/one-bond coupling at which maximum/minimum transfer amplitudes $^{n/1}a_{\max/\min}$ occur; $^{n/1}a$, mean amplitude over entire long-range/one-bond coupling array.

TABLE 2

Delay Sets and Performance Characteristics for *Ultra* and Broadband MBOB Optimized for a Lorentzian Linewidth of 1 Hz

No.	Δ_1 [ms]	Δ_2 [ms]	Δ_3 [ms]	Δ_4 [ms]	[$^nJ_{90\%}$]	[$^nJ_{75\%}$]	[$^nJ_{50\%}$]	[$^nJ_{25\%}$]	a_{90}	a_{75}	a_{50}	a_{25}	^nJ(max)	$^na_{\max}$	^nJ(min)	$^na_{\min}$	^na	^1J(max)	$^1a_{\max}$	^1J(max)	$^1a_{\min}$	^1a
1	*273.0*	*232.8*	*195.6*	*173.4*	0.03 2.20	0.03 2.80	0.03 3.47	0.03 17.10	0.29	0.33	0.34	0.31	2.27	0.47	40.37	0.13	0.28	168.02	0.37	221.64	0.05	0.22
2	230.3	196.5	164.5	161.4	0.47 2.70	0.03 3.37	0.03 4.10	0.03 12.13	0.39	0.37	0.38	0.34	2.63	0.53	30.40	0.05	0.30	147.51	0.38	221.36	0.09	0.24
3	110.1	108.1	106.3	90.1	2.43 5.60	1.27 6.57	0.03 7.73	0.03 8.70	0.64	0.58	0.50	0.48	4.80	0.69	9.27	0.11	0.39	156.75	0.45	222.48	0.15	0.31
4	99.3	98.3	96.7	95.1	2.67 6.07	1.47 7.10	0.03 8.30	0.03 9.30	0.66	0.61	0.51	0.49	5.13	0.71	10.20	0.03	0.41	143.80	0.44	225.00	0.14	0.32
5	97.4	80.0	67.8	59.0	3.97 7.37	2.43 8.83	0.03 11.13	0.03 49.97	0.70	0.65	0.52	0.44	6.37	0.73	49.97	0.20	0.43	134.84	0.53	211.84	0.16	0.34
6	97.9	80.5	58.8	55.4	4.33 7.30	2.67 8.97	0.37 15.80	0.03 49.97	0.69	0.64	0.51	0.44	6.53	0.72	49.97	0.17	0.44	163.61	0.51	225.00	0.17	0.35
7	75.3	72.5	49.1	46.3	5.33 9.03	3.43 10.93	1.20 13.00	0.03 39.53	0.73	0.68	0.59	0.49	7.87	0.75	40.73	0.11	0.45	148.21	0.52	213.80	0.17	0.36
8	90.7	72.1	55.1	32.6	— —	3.50 9.53	1.17 27.60	0.03 49.97	—	0.64	0.52	0.46	7.20	0.69	33.07	0.29	0.46	178.94	0.54	225.00	0.12	0.36
9	67.0	58.6	46.2	40.7	6.13 10.70	4.10 12.73	1.70 15.50	0.03 49.97	0.75	0.70	0.61	0.46	9.03	0.78	44.77	0.26	0.46	150.73	0.64	213.31	0.19	0.37
10	44.8	41.1	31.9	28.7	9.27 15.90	6.47 18.77	3.27 22.00	0.03 49.97	0.79	0.74	0.66	0.48	13.00	0.81	24.33	0.35	0.48	150.94	0.52	225.00	0.18	0.39
11	46.4	39.8	31.5	28.4	9.37 15.77	6.50 18.70	3.27 23.47	0.03 49.97	0.79	0.74	0.64	0.49	12.97	0.81	31.73	0.38	0.49	150.94	0.60	225.00	0.17	0.39
12	49.1	35.6	32.3	23.4	10.47 15.00	6.97 18.67	3.50 27.97	0.03 49.97	0.77	0.72	0.61	0.49	13.13	0.78	40.73	0.34	0.49	163.47	0.60	225.00	0.23	0.39
	65	65	65	65	4.57 9.40	3.03 10.83	0.90 12.57	0.03 14.00	0.75	0.70	0.60	0.54	7.63	0.79	30.77	0.00	0.44	153.88	0.66	192.31	0.00	0.35
	100	100	100	100	2.57 5.90	1.40 6.90	0.03 8.07	0.03 9.03	0.66	0.60	0.51	0.49	5.00	0.71	10.00	0.00	0.40	159.97	0.59	225.00	0.00	0.31

Note. Δ_i, delays in ms; [$^nJ_{x\%}$], left-most intervals in which at least $x\%$ of the maximal transfer amplitude is actually achieved; a_x, mean in the respective interval; $^{n/1}J$(max/min), long-range/one-bond coupling at which maximum/minimum transfer amplitudes $^{n/1}a_{\max/\min}$ occur; $^{n/1}a$, mean amplitude over entire long-range/one-bond coupling array.

TABLE 3

Delay Sets and Performance Characteristics for *Ultra* and Broadband MBOB Optimized for a Lorentzian Linewidth of 2 Hz

No.	Δ_1 [ms]	Δ_2 [ms]	Δ_3 [ms]	Δ_4 [ms]	[$^nJ_{90\%(95\%)}$]	[$^nJ_{75\%}$]	[$^nJ_{50\%}$]	[$^nJ_{25\%}$]	a_{90}	a_{75}	a_{50}	a_{25}	^nJ(max)	$^na_{max}$	^nJ(min)	$^na_{min}$	^na	^1J(max)	$^1a_{max}$	^1J(max)	$^1a_{min}$	^1a
1	*181.1*	*160.0*	*115.0*	*99.3*	0.03 2.90 (2.17)	0.03 4.03	0.03 5.30	0.03 10.03	0.20	0.25	0.27	0.25	3.57	0.37	49.97	0.08	0.23	149.47	0.30	196.09	0.04	0.18
2	121.5	119.0	116.2	112.8	0.03 4.23	0.03 5.27	0.03 6.50	0.03 7.50	0.28	0.31	0.32	0.31	4.27	0.45	8.43	0.03	0.26	149.19	0.28	218.07	0.08	0.20
3	110.7	107.5	98.2	95.2	0.03 5.03	0.03 6.17	0.03 7.50	0.03 8.63	0.31	0.34	0.35	0.34	4.83	0.49	9.30	0.09	0.28	155.49	0.30	218.91	0.08	0.22
4	116.2	107.8	89.5	72.5	0.80 5.17	0.03 6.47	0.03 7.97	0.03 49.97	0.36	0.35	0.36	0.29	5.10	0.50	43.03	0.17	0.29	165.78	0.38	218.00	0.07	0.23
5	96.7	84.4	81.8	80.8	1.50 6.27	0.03 7.57	0.03 9.10	0.03 10.53	0.44	0.38	0.39	0.37	5.80	0.54	12.20	0.09	0.31	145.55	0.37	225.00	0.12	0.25
6	57.4	54.7	53.1	50.7	4.53 10.83	2.27 12.67	0.03 14.90	0.03 16.77	0.61	0.55	0.47	0.45	9.17	0.66	18.30	0.08	0.39	153.11	0.40	217.72	0.15	0.30
7	58.1	55.0	52.5	49.8	4.57 10.83	2.27 12.70	0.03 14.93	0.03 16.80	0.61	0.55	0.47	0.45	9.17	0.66	18.20	0.10	0.39	157.73	0.41	215.13	0.15	0.30
8	62.7	52.6	50.2	41.3	5.03 10.90	2.63 13.00	0.03 15.40	0.03 49.97	0.61	0.56	0.47	0.38	9.43	0.66	19.03	0.22	0.38	173.97	0.46	225.00	0.16	0.30
9	71.0	54.6	45.4	32.2	5.87 9.63	2.97 12.33	0.03 18.23	0.03 49.97	0.59	0.54	0.45	0.39	9.23	0.62	42.27	0.27	0.39	152.83	0.48	209.25	0.15	0.31
10	57.7	54.7	36.4	32.9	6.53 11.50	3.67 14.20	0.03 17.20	0.03 49.97	0.62	0.57	0.47	0.42	10.40	0.65	34.67	0.23	0.42	159.69	0.44	225.00	0.15	0.32
11	48.6	41.0	40.0	38.1	6.63 14.07	4.03 16.47	0.03 19.27	0.03 23.10	0.66	0.61	0.50	0.47	11.67	0.70	25.00	0.14	0.41	148.70	0.48	216.04	0.16	0.33
12	38.6	30.8	27.2	23.2	10.63 19.00	6.97 22.63	2.47 29.20	0.03 49.97	0.70	0.65	0.55	0.43	15.73	0.72	36.77	0.29	0.43	157.94	0.48	225.00	0.20	0.35
13	46.0	31.6	28.6	15.0	— —	7.43 19.37	2.57 49.97	0.03 49.97	—	0.61	0.47	0.45	14.43	0.65	4.97	0.34	0.45	132.32	0.53	225.00	0.12	0.36
14	34.2	31.5	23.9	22.3	11.43 20.53	7.60 24.33	2.97 28.67	0.03 49.97	0.71	0.66	0.57	0.44	16.80	0.73	41.83	0.30	0.44	169.42	0.49	225.00	0.18	0.36
15	32.1	22.8	18.9	15.0	16.67 22.63	10.60 29.03	4.87 49.97	0.03 49.97	0.70	0.65	0.52	0.48	19.97	0.70	4.97	0.27	0.48	126.37	0.47	225.00	0.18	0.38
	65	65	65	65	3.27 8.80	0.70 10.40	0.03 12.27	0.03 13.87	0.56	0.47	0.45	0.43	7.63	0.62	30.77	0.00	0.35	153.88	0.52	192.31	0.00	0.28
	100	100	100	100	0.03 5.23	0.03 6.40	0.03 7.73	0.03 8.90	0.32	0.35	0.36	0.34	5.00	0.50	10.00	0.00	0.28	159.97	0.42	225.00	0.00	0.22

Note. Δ_i, delays in ms; [$^nJ_{x\%}$], left-most intervals in which at least $x\%$ of the maximal transfer amplitude is actually achieved; a_x, mean in the respective interval; $^{n/1}J$(max/min), long-range/one-bond coupling at which maximum/minimum transfer amplitudes $^{n/1}a_{max/min}$ occur; $^{n/1}a$, mean amplitude over entire long-range/one-bond coupling array.

TABLE 4

Delay Sets and Performance Characteristics for *Ultra* and Broadband MBOB Optimized for a Lorentzian Linewidth of 3 Hz

No.	Δ_1 [ms]	Δ_2 [ms]	Δ_3 [ms]	Δ_4 [ms]	[$^nJ_{90\%(98\%)}$]	[$^nJ_{75\%}$]	[$^nJ_{50\%}$]	[$^nJ_{25\%}$]	a_{90}	a_{75}	a_{50}	a_{25}	^nJ(max)	$^na_{max}$	^nJ(min)	$^na_{min}$	^na	^1J(max)	$^1a_{max}$	^1J(max)	$^1a_{min}$	^1a
1	*106.6*	*101.6*	*81.5*	*77.6*	0.03 4.83 (3.10)	0.03 6.37	0.03 8.10	0.03 11.40	0.21	0.25	0.27	0.24	5.40	0.38	38.63	0.08	0.22	168.72	0.28	201.76	0.04	0.17
2	*97.4*	*89.4*	*87.2*	*72.0*	0.03 5.37	0.03 6.90	0.03 8.67	0.03 10.17	0.23	0.27	0.28	0.27	5.73	0.40	11.20	0.10	0.23	124.41	0.27	200.71	0.08	0.18
3	80.0	72.2	70.4	63.3	0.03 7.10	0.03 8.80	0.03 10.77	0.03 12.43	0.29	0.32	0.33	0.32	6.93	0.46	13.87	0.09	0.26	139.95	0.33	218.77	0.09	0.21
4	80.0	67.4	65.2	63.7	0.03 7.40	0.03 9.13	0.03 11.17	0.03 13.37	0.30	0.33	0.34	0.32	7.17	0.47	15.33	0.09	0.27	137.71	0.32	225.00	0.11	0.21
5	50.6	50.5	48.9	47.6	3.63 11.37	0.03 13.50	0.03 16.03	0.03 18.20	0.49	0.40	0.41	0.39	10.00	0.57	19.83	0.04	0.32	141.77	0.40	225.00	0.11	0.26
6	49.3	48.1	46.1	45.4	4.07 11.97	0.03 14.17	0.03 16.83	0.03 19.03	0.51	0.41	0.41	0.40	10.43	0.58	20.80	0.05	0.32	148.35	0.37	225.00	0.14	0.26
7	48.5	46.1	44.8	41.3	4.53 12.53	0.03 14.87	0.03 17.60	0.03 19.93	0.52	0.42	0.42	0.40	10.90	0.59	21.70	0.08	0.33	149.40	0.38	225.00	0.14	0.27
8	63.3	49.5	46.4	31.9	4.60 10.50	0.03 13.17	0.03 17.23	0.03 49.97	0.49	0.39	0.39	0.33	10.00	0.54	43.10	0.24	0.33	157.17	0.41	225.00	0.13	0.27
9	73.1	54.6	36.8	32.7	5.17 8.73	0.03 12.07	0.03 23.37	0.03 49.97	0.46	0.36	0.38	0.34	9.53	0.51	27.37	0.18	0.34	162.91	0.41	225.00	0.09	0.26
10	56.8	48.9	32.1	30.9	6.07 11.67	2.07 14.87	0.03 27.83	0.03 49.97	0.52	0.45	0.40	0.35	11.20	0.56	35.20	0.19	0.35	160.04	0.48	202.46	0.15	0.28
11	36.5	35.4	32.8	32.6	7.33 17.10	3.87 20.00	0.03 23.47	0.03 26.37	0.60	0.54	0.46	0.44	14.20	0.64	28.27	0.09	0.39	160.25	0.40	225.00	0.14	0.29
12	39.3	30.9	28.2	19.3	10.20 17.73	5.80 21.93	0.03 29.80	0.03 49.97	0.60	0.55	0.44	0.40	15.77	0.63	49.97	0.26	0.40	153.25	0.47	225.00	0.15	0.31
13	33.6	31.6	23.4	22.4	10.43 20.27	6.27 24.20	0.03 28.70	0.03 49.97	0.62	0.57	0.47	0.39	16.97	0.65	42.73	0.26	0.39	126.93	0.46	225.00	0.16	0.32
14	31.9	29.9	22.6	14.9	13.20 20.23	7.83 25.50	0.73 30.90	0.03 49.97	0.62	0.57	0.47	0.42	18.13	0.63	4.97	0.27	0.42	131.83	0.52	225.00	0.17	0.34
	65	65	65	65	0.03 8.13	0.03 9.90	0.03 11.97	0.03 13.70	0.32	0.35	0.35	0.34	7.63	0.49	30.77	0.00	0.27	153.88	0.42	192.31	0.00	0.22
	100	100	100	100	0.03 4.37 (2.90)	0.03 5.77	0.03 7.37	0.03 8.70	0.19	0.23	0.25	0.24	5.00	0.36	10.00	0.00	0.20	159.97	0.30	225.00	0.00	0.16

Note. Δ_i, delays in ms; [$^nJ_{x\%}$], left-most intervals in which at least $x\%$ of the maximal transfer amplitude is actually achieved; a_x, mean in the respective interval; $^{n/1}J$(max/min), long-range/one-bond coupling at which maximum/minimum transfer amplitudes $^{n/1}a_{max/min}$ occur; $^{n/1}a$, mean amplitude over entire long-range/one-bond coupling array.

ethylene groups, and 25 Hz in aldehydes, while in trichloroacetaldehyde or ethyne, they may amount up to approximately 50 Hz (*11*).

However, even by putting extreme weights ($w = 100$) onto the low end of the ^nJ domain, the fitting algorithms did not provide parameters allowing coherence transfer via ^nJ coupling constants in the range from 0.1 to 1–3 Hz to be observed with 90%, 95%, or even 98% of the maximum intensity without gaps for larger ^nJ's. Such delay sets for *ultra* experiments can be obtained by subjecting the above fitting results to the following refinement steps:

(i) Increment each of the delays $\{\Delta_1, \Delta_2, \ldots, \Delta_N\}$ in random order by some $\delta\Delta = 2$ ms until 90% of the maximum intensity is achieved in an interval of the long-range coupling constants reaching from 0.03 up to 1.2 Hz for a Lorentzian linewidth of 0.5 Hz. (Likewise, at 1-Hz linewidth 90% can be reached from 0.03 to 2.2 Hz; at 2(3) Hz linewidth it is 95% (98%) of the maximum between 0.03 Hz and 2.17(3.10) Hz, respectively.)

(ii) While maintaining 90% (or 95%, or 98%) intensity in the interval of interest, shift the delays by a dynamic step size $\pm\delta\Delta$' to recursively obtain larger values of minimum amplitude in the higher ^nJ domain.

(iii) Shift delays analogously, yet by smaller increments $\pm\varepsilon\Delta$ to refine the ^1J domain while keeping the amplitudes in the long-range part.

Moreover, because the refinement procedure for the *ultra* experiments in the ^1J domain does not compromise the ^nJ part, the *ultra* delay sets can equally well be used for *ultra*-HMBC and *ultra*-XLOC experiments.

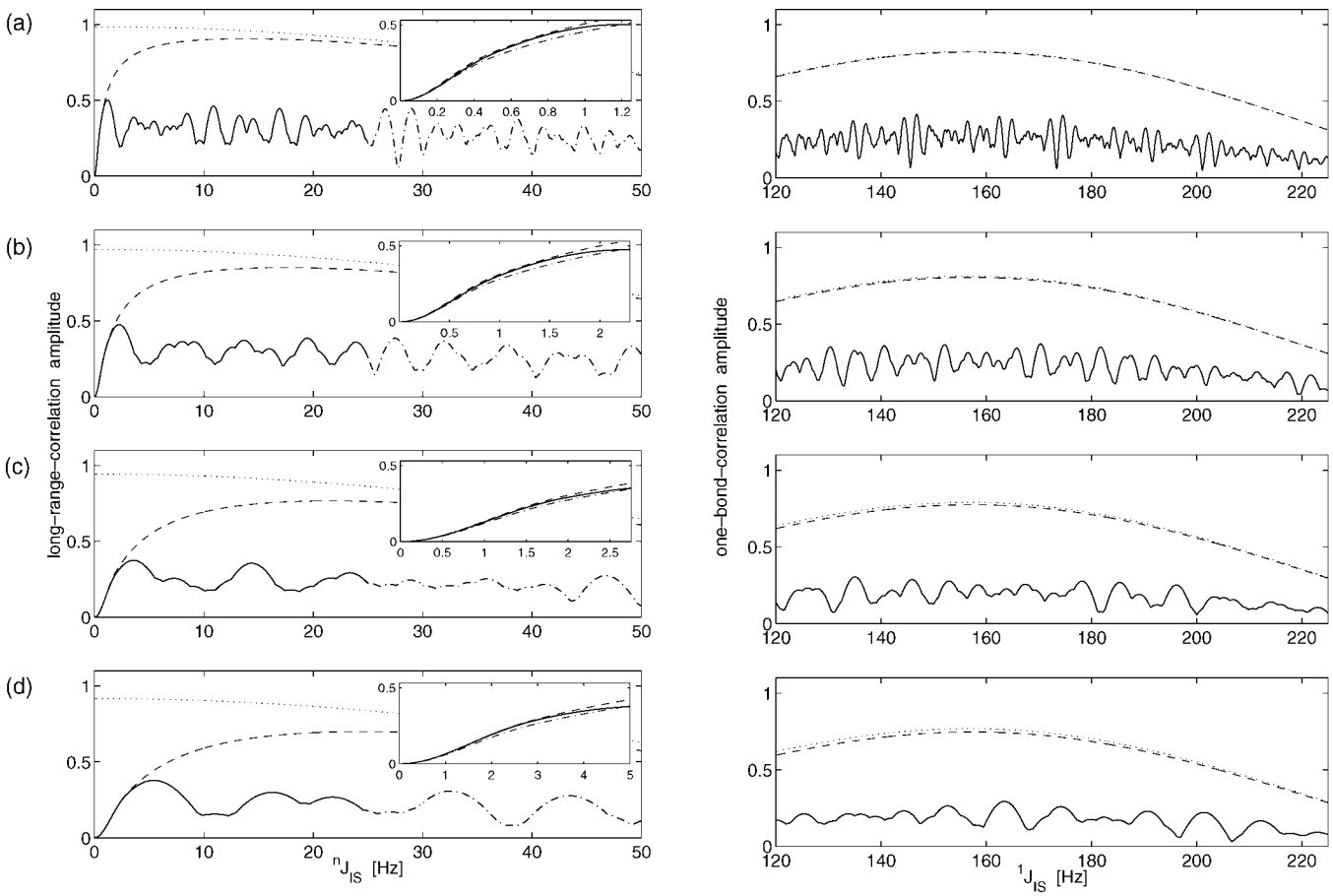

FIG. 3. Performance of the *ultra*-MBOB experiments optimized for high sensitivity at very small long-range coupling constants. The left traces show the signal amplitudes of the long-range correlation part, whereas the right ones represent the one-bond correlation intensities. The solid lines denote the normalized transfer amplitudes in the ranges subjected to the optimization procedure described in the text, while the dash-dotted part continues the signal amplitudes beyond that range. The dotted lines give the characteristics of the third-order low-pass vs high-pass *J* filter used to separate the long-range and the one-bond correlations. In the insets, the dashed curve indicates the maximum achievable effective normalized signal amplitudes (Eq. [8]) times the filter function (dotted lines) if all the four delays are set according to Eq. [2], while the dash-dotted line gives 90% of it. (a) Characteristics of *ultra*-MBOB assuming a proton linewidth of 0.5 Hz. The delays are Δ [ms] = 501.5, 432.8, 397.9, 323.5 (see first row in Table 1). (b) Performance of *ultra*-MBOB in the case of 1-Hz proton linewidth with the delays Δ [ms] = 273.0, 232.8, 195.6, 173.4 taken from Table 2. (c) Same for *ultra*-MBOB with 2-Hz proton linewidth. The delays Δ [ms] = 181.1, 160.0, 115.0, 99.3 can be found in Table 3. (d) Same for *ultra*-MBOB for 3-Hz proton linewidth with the delays Δ [ms] = 106.6, 101.6, 81.5, 77.6 (Table 4).

RESULTS

Representative sets of delays Δ resulting from the fitting procedures above are given in Tables 1 through 4 corresponding to the linewidths 0.5, 1, 2, and 3 Hz, respectively. To this end, the standard Simplex algorithm (*12*) within the MATLAB package (*13*) was used. It is convenient to characterize the results according to the following criteria: (1) the long-range J interval covered, (2) position of the first maximum of the long-range intensity function, (3) minimum intensities in percent of the theoretical maximum (Eq. [8]) in the J ranges covered. To serve point (1), intervals $[{}^nJ^{\min}, {}^nJ^{\max}]$ are indicated within which at least 90%, 75%, 50%, and 25% of the respective maximum achievable signal amplitude are actually obtained (details in the table captions). (2) ${}^nJ$ values for maximum and minimum amplitudes are given as well as the mean intensity. (3) The ${}^1J$ domain obtained in the one-bond correlation part is characterized in the same way.

Parameters for the *ultra* experiments are indicated in italics and displayed in the first lines, respectively. They result from subjecting the top-30 results of clustered best fits (to the target function parameterized by $w = 20$, ${}^nJ^{\max} = 25$ Hz (Eq. [11]) to 1000 different refinement steps (i) consisting of 5000 internal iterations each. The results with highest minimum signal amplitude in the range of 2 to 25 Hz are further refined by 5000 iterations of steps (ii) and (iii), respectively. Note that the range of 90% maximal signal intensity extends from a coupling constant as low as ${}^nJ = 0.03$ Hz to over 1 Hz (linewidth of 0.5 Hz), 2 Hz (1- and 2-Hz linewidths), and 3 Hz (3-Hz linewidth) without introducing severe gaps in the higher end of ${}^nJ$'s.

For various linewidths, the performance of *ultra* experiments is displayed in Fig. 3, while examples of broadband MBOB experiments are shown in Fig. 4.

It follows from the intensity function in Eq. [1] that it is possible to fine-tune the values in Tables 1–4 in order to suit slightly different J ranges: A scaling of all the delays Δ_i in a set by a factor $1/k$ will to a good approximation scale the J ranges covered by k. The relation is exact for the factor $\sin(\pi J \Delta)$, but only for narrow ranges of delays Δ does it approximately amount to

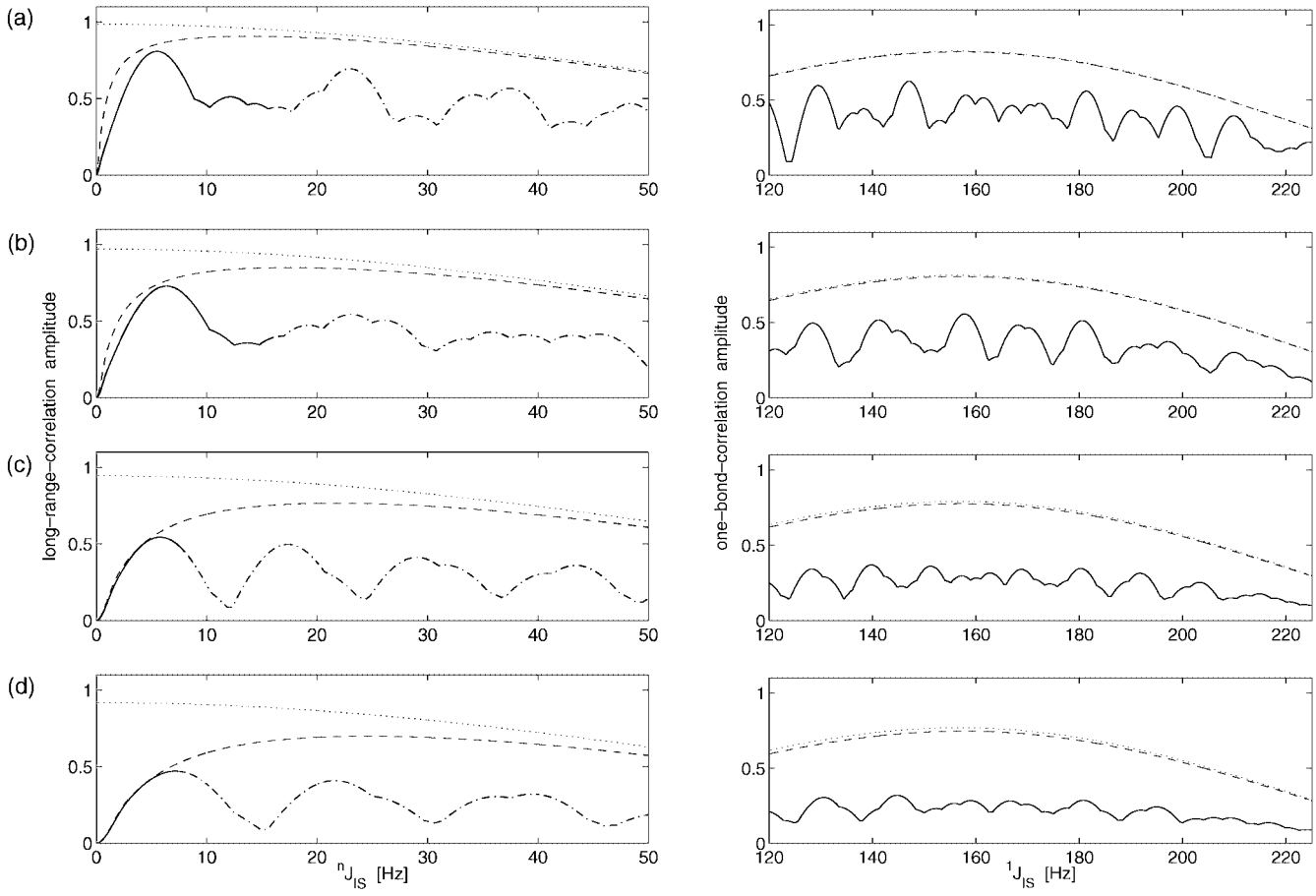

FIG. 4. Performance of broadband MBOB experiments. Again, the left traces show the signal amplitudes of the long-range correlation part, while the right ones display the one-bond correlation intensities. Line types as in Fig. 3. (a) For a Lorentzian linewidth of 0.5 Hz, the delays (taken from Table 1, row 5) are $\Delta = 112.6$, 97.3, 73.0, and 64.2 ms. (b) Lorentzian linewidth of 1 Hz. Delays are $\Delta = 97.4$, 80.0, 67.8, and 59.0 ms (Table 2, row 5). (c) Linewidth 2 Hz. The delays are $\Delta = 96.7$, 84.4, 81.8, and 80.8 ms (Table 3, row 5). (d) The 3-Hz proton linewidth. The delay set $\Delta = 80.0$, 67.4, 65.2, and 63.7 ms is taken from Table 4, row 4.

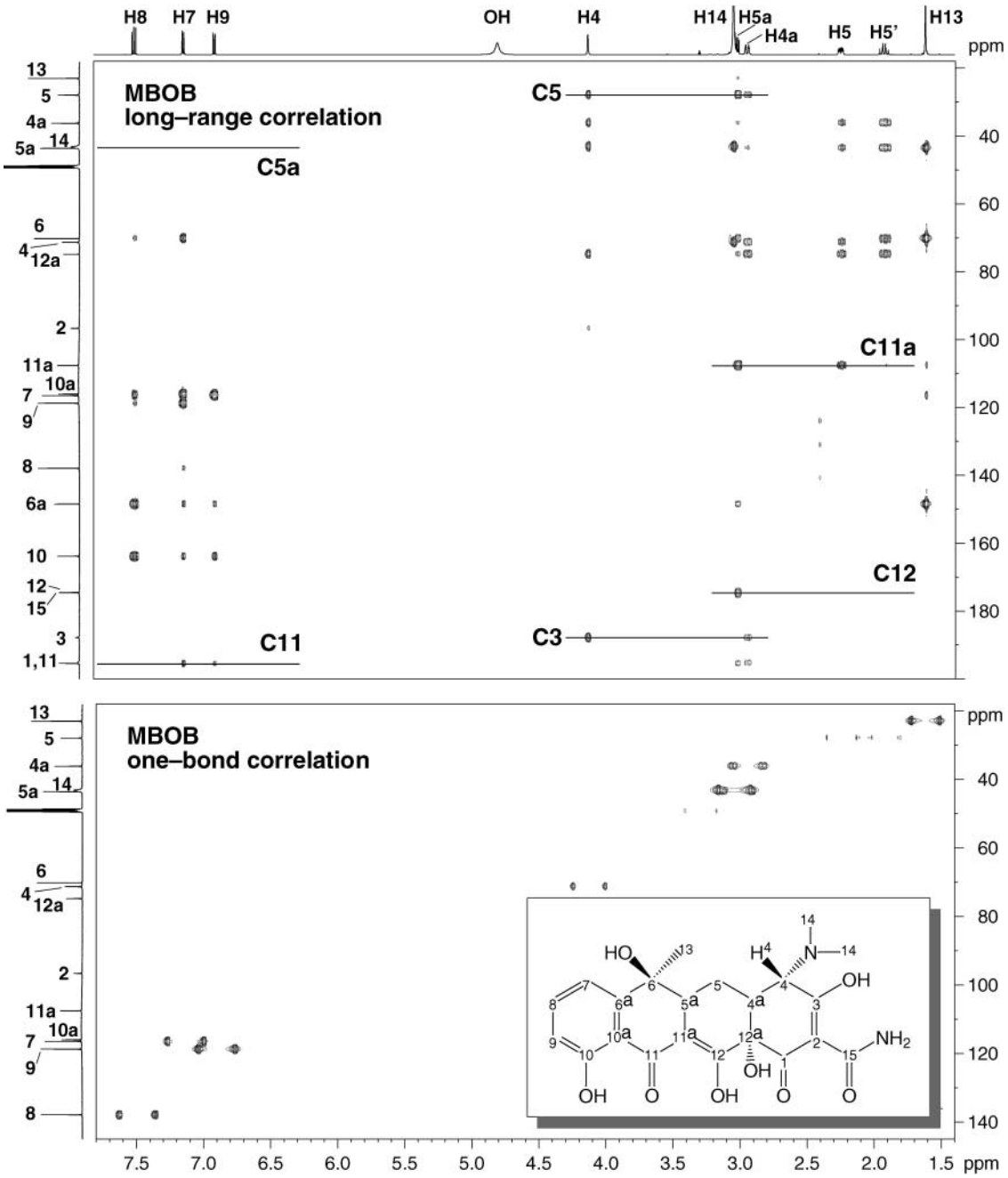

FIG. 5. MBOB spectra of 60 mg tetracycline hydrochloride in 600 μl CD_3OD recorded at 300 K with the pulse sequence in Fig. 1a on a Bruker DRX 600 MHz spectrometer. A third-order J filter was applied. Parameters: relaxation delay 2.4 s; $\tau_1 = 3.91$ ms, $\tau_2 = 3.45$ ms, $\tau_3 = 3.08$ ms (i.e., $J^{\min} = 125$ Hz and $J^{\max} = 165$ Hz); $\Delta = 97.4$, 80.0, 67.8, and 59.0 ms (see Table 2, row 5, and Fig. 4b); $t_1(\max) = 4.21$ ms; $t_2(\max) = 376.7$ ms; 8 scans per Δ value. Sine-shaped gradients of 1.0-ms duration and a unit strength of 5.0×10^{-2} T/m followed by a gradient recovery delay of 0.3 ms were applied. Two data sets, *even* and *odd*, were recorded and combined as described in the caption to Fig. 1a. Data matrices of 256×4096 points covering 30189×5435 Hz were zero-filled to 1024×4096 prior to Fourier transformation and the window functions were a cosine in t_1 and a sine shifted by $\pi/3$ in t_2. MBOB long-range correlation spectrum (top) resulting from addition of the two data sets (*even* + *odd*). MBOB one-bond correlation spectrum (bottom) resulting from subtraction of the two data sets (*even* − *odd*). The signals are split by $^1J_{CH}$ in the F_2 dimension. Single pulse 1D ^{1}H and ^{13}C spectra with 64 and 512 scans, respectively, are printed as projections next to the 2D spectra. Indicated 1D traces are shown in Fig. 6.

a scaling factor in the exponential term. Nevertheless, this fine-tuning procedure is of good use in practical work with MBOB, broadband HMBC, and broadband XLOC.

EXPERIMENTAL VERIFICATION

For demonstration, MBOB and HMBC spectra were recorded for two samples: (i) tetracycline in solution phase exhibiting a proton linewidth of 1 Hz to best approximation, and (ii) a tetrapeptide assembled on a SPOCC-1500 resin (*14*) under HR-MAS conditions thus showing a proton linewidth of about 3 Hz. Figure 5 displays 600-MHz MBOB long-range (top) and MBOB one-bond (bottom) correlation spectra of tetracycline hydrochloride in d4-methanol using the delays $\Delta =$ 97.4, 80.0, 67.8, and 59.0 ms (see Table 2, row 5) as illustrated in Fig. 4b. Besides all the ^2J and ^3J correlations, also some ^4J and even ^5J correlations are observed in the long-range correlation spectrum. Moreover, here the MBOB-typical splitting of the cross peaks by ^1J in the F_2 dimension of the one-bond correlation spectrum is very useful for the assignment of the H,C 14 and H,C 5a resonances: both the proton ($\delta_{14} = 3.05$ ppm; $\delta_{5a} = 3.02$ ppm) and carbon ($\delta_{14} = 43.17$ ppm; $\delta_{5a} = 43.48$ ppm) chemical shifts are very similar so that unique assignment is difficult based on a conventional HSQC spectrum (not shown). In the MBOB one-bond correlation spectrum, however, the left multiplet component exhibits resonances clearly separated due to differences in the ^1J coupling constant ($^1J_{(14)} = 141$ Hz; $^1J_{(5a)} = 125$ Hz).

Figure 6 displays the sections indicated in Fig. 5: (a) MBOB for 1-Hz linewidth, $\Delta = 97.4$, 80.0, 67.8, and 59.0 ms (see Table 2, row 5), (b) *ultra*-MBOB for 1-Hz linewidth, $\Delta = 273.0$, 232.8, 195.6, and 173.4 ms (see Table 2, row 1), the characteristics of which are illustrated in Fig. 3b; for comparison (c) shows an HMBC spectrum with $\Delta = 65$ ms and (d) gives an HMBC spectrum with $\Delta = 100$ ms each with equal total experimental time. In the *ultra*-MBOB spectrum (b) it is possible to observe correlations via very small J coupling constants like $^5J_{(H8,C11)}$, $^4J_{(H5',C12)}$, and $^5J_{(H8,C5a)}$, which are not accessible by conventional MBOB (a), or 65-ms HMBC (c). Some of these

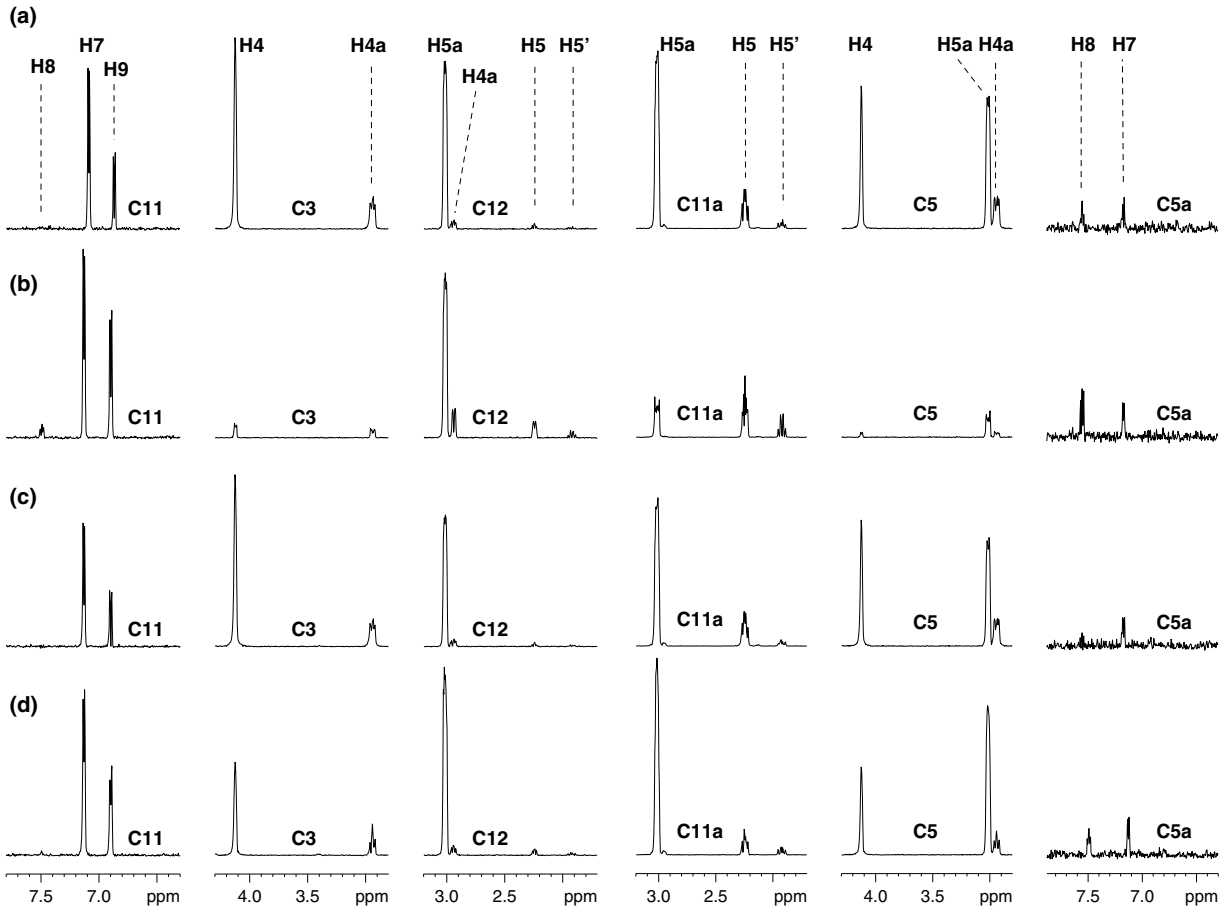

FIG. 6. The 1D sections as indicated in Fig. 5 from (a) MBOB long-range correlation spectrum $\Delta = 97.4$, 80.0, 67.8, and 59.0 ms (Table 2, row 5); (b) *ultra*-MBOB long-range correlation spectrum, same parameters and processing as (a) except $\Delta = 273.0$, 232.8, 195.6, and 173.4 ms (Table 1, row 1); (c) HMBC spectrum recorded with the same parameters as (a) except $\Delta = 65$ ms and 64 scans to achieve equal numbers of scans for each FID in the resulting data set; (d) HMBC spectrum recorded with the same parameters as (c) except $\Delta = 100$ ms (compare Table 2, rows 13 and 14, respectively).

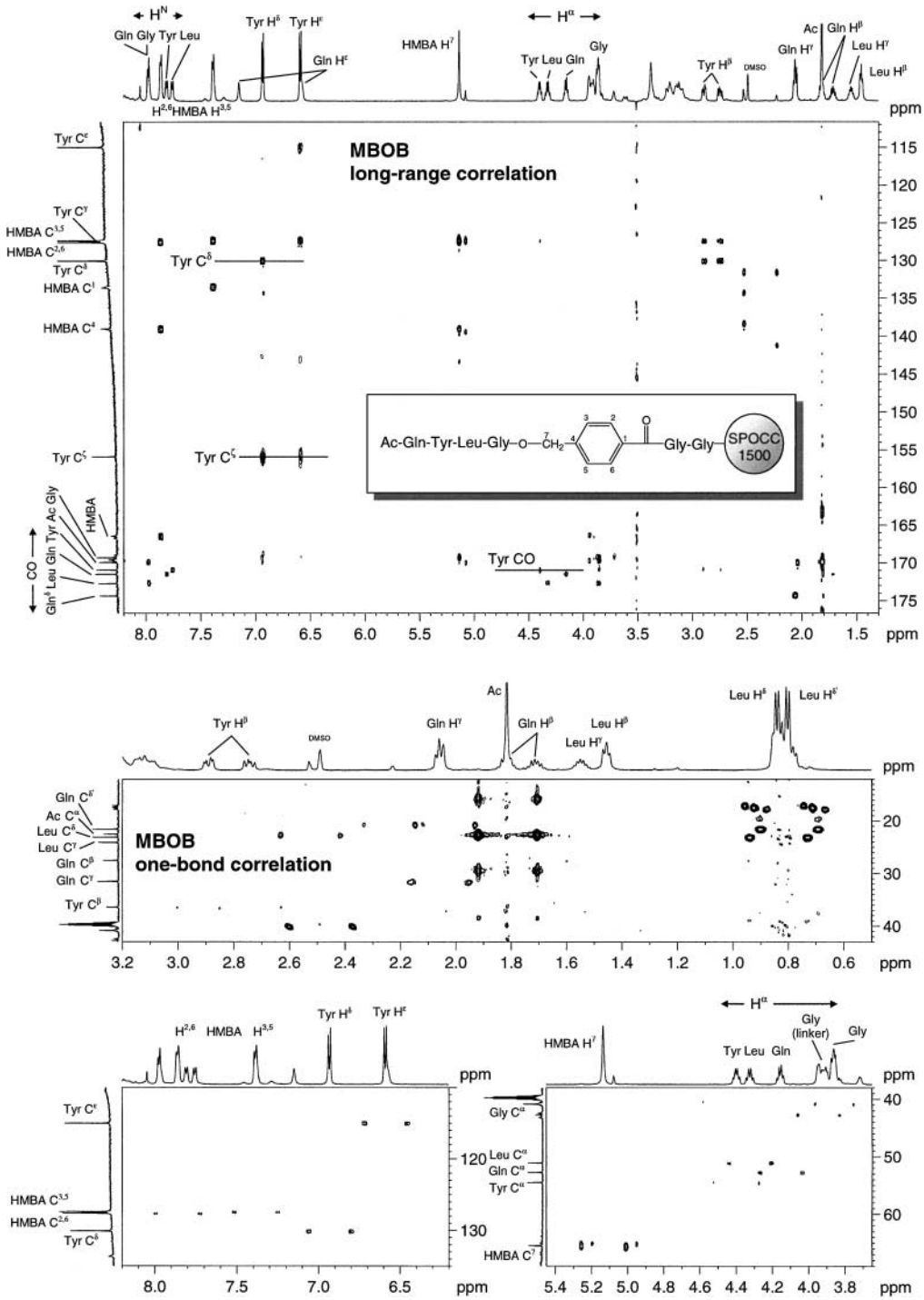

FIG. 7. Excerpt of HR-MAS MBOB long-range correlation spectrum of Ac-Gln-Tyr-Leu-Gly-HMBA-Gly-Gly assembled on SPOCC-1500, swollen in $d6$-DMSO and recorded at 300 K with the pulse sequence in Fig. 1a on a Bruker DRX 600 MHz spectrometer. Sample volume was 50 μl using a ZrO_2 rotor with PTFE spacer with spinning speed of 4800 Hz. A third-order J filter was applied. Parameters: relaxation delay 2.0 s with presaturation of the main resin signal, $\gamma B_1 =$ 33 Hz; $\tau_1 = 3.89$ ms, $\tau_2 = 3.33$ ms, $\tau_3 = 2.92$ ms (i.e., $J^{\min} = 125$ Hz and $J^{\max} = 175$ Hz); $\Delta = 80.0$, 67.4, 65.2, and 63.7 ms (see Table 4, row 4); $t_1(\max) =$ 5.81 ms; $t_2(\max) = 526.0$ ms; 32 scans per Δ value. Sine-shaped gradients of 1.25-ms duration and a unit strength of 0.3 T/m followed by a gradient recovery delay of 0.3 ms were applied. Two data sets, *even* and *odd*, were recorded and combined as described in the caption to Fig. 1a. Data matrices of 300×4096 points covering 25657.5×7788.2 Hz were linear predicted to 600×4096 points using 80 coefficients in the t_1 dimension and zero-filled to 2048×4096 prior to Fourier transformation and the window functions were a cosine in t_1 and a sine shifted by $\pi/3$ in t_2. The MBOB long-range correlation spectrum (top) was obtained by addition of the two data sets (i.e., *even* + *odd*). Excerpts from the MBOB one-bond correlation spectrum are shown at the bottom and were obtained by subtraction of the two data sets (*even* − *odd*). Single pulse 1D ^{1}H and ^{13}C spectra with 64 and 1024 scans, respectively, are printed as projections next to the 2D spectra. Indicated 1D traces are shown in Fig. 8.

correlations are also visible in the 100-ms HMBC (d), but the intensity is generally lower as compared to *ultra*-MBOB (b) as also seen for $^3J_{(H4a,C12)}$, $^3J_{(H5,C11a)}$, and $^3J_{(H5',C11a)}$. In contrast, for larger coupling constants, the *ultra*-MBOB spectrum shows less intensity than the 100-ms HMBC which is not as sensitive as the 65-ms HMBC in this range, as can be seen in the cross peaks due to $^2J_{(H4,C3)}$ and $^2J_{(H4a,C5)}$. The low intensity for the $^2J_{(H4,C3)}$ and $^3J_{(H4,C5)}$ cross peaks in the *ultra*-MBOB spectrum is due to the homonuclear $^4J_{(H4,H14)}$ of 1.5 Hz that evolves during the long Δ delays. In practice, the problem of unresolved ^{1}H–^{1}H coupling constants of this type can be considered in terms of an effective T_2 relaxation time. In other words, the correlations involving H4 would benefit from application of Δ delays optimized not for a 1-Hz linewidth but for a larger value. Here the conventional MBOB experiment (a) combines the pros of the 65-ms and 100-ms HMBC, which otherwise both would have to be recorded separately in order to get reliable information. In $^2J_{(H4,C3)}$, for example, MBOB (a) is similar to a 65-ms HMBC (c), which in turn is more sensitive than 100-ms HMBC (d), and for $^3J_{(H5a,C12)}$ MBOB (a) has similar intensity as the 100-ms HMBC (d), which in this case is more sensitive than 65-ms HMBC (c).

Figure 7 shows excerpts of 600-MHz MBOB long-range and one-bond correlation HR-MAS spectra, respectively, with the delays set for a 3-Hz proton linewidth. It is run on the resin-bound (SPOCC-1500 resin using a HMBA-Gly-Gly linker) tetrapeptide Ac-Gln-Tyr-Leu-Gly swollen in *d*6-DMSO. All the ^2J and ^3J correlations necessary for a complete sequential assignment are observed in the long-range correlation spectrum.

As is evident from Fig. 2a, a 3-Hz linewidth is close to the border where a single delay becomes adequate. However, even at this linewidth MBOB is preferable because of the absence of blind spots over the relevant J range. By virtue of the relatively flat nature of the $\Delta_m(J, 3\text{ Hz})$ function (see Fig. 2a) the MBOB delays are in a narrow range ($\Delta = 80.0$, 67.4, 65.2, and 63.7 ms) giving rise to the performance pattern shown in Fig. 4d. If only HMBC were to be run, one would typically record a spectrum with $\Delta = 65$ ms or one with $\Delta = 100$ ms. The smallest J's are below optimum sensitivity for $\Delta = 65$ ms, but they exhibit highest sensitivity for $\Delta = 100$ ms as illustrated in the first column of Fig. 8 for traces from (a) MBOB for 3-Hz linewidth, $\Delta = 80.0$, 67.4, 65.2, and 63.7 ms (see Table 4, row 4) (b) *ultra*-MBOB for 3-Hz linewidth, $\Delta = 106.6$, 101.6, 81.5, 77.6 ms (see Table 4, row 1 and Fig. 3d); (c) HMBC $\Delta = 65$ ms; and (d) HMBC $\Delta = 100$ ms. However, this advantage comes at severe costs: for long-range coupling constants around 10 Hz as in the case of $^3J_{(H\delta,C\delta)}$ and $^3J_{(H\delta,C\zeta)}$ in tyrosine, the cross peaks almost vanish in the $\Delta = 100$ ms HMBC spectrum (d) due to a blind spot for this size of J. Conventional solutions to this problem would be to live with a compromise delay around, e.g., $\Delta \approx 80$ ms or to add HMBC spectra recorded with $\Delta = 65$ ms and $\Delta = 100$ ms in absolute value giving a spectrum similar to the *ultra* MBOB correlation shown in Fig. 8. However, these simple solutions would be inadequate for uniformity in the one-bond correlation spectrum and unfavorable in the long-range correlation. Either alternative does not show the MBOB benefit of covering both the *long-range* and the *one-bond J* region simultaneously: Undesirable blind spots in both regions occur in case of single compromise delays, and the combination of $\Delta = 65$ ms and $\Delta = 100$ ms entails unattractively low amplitudes in the one-bond correlation spectrum at coupling constants between 135 and 140 Hz.

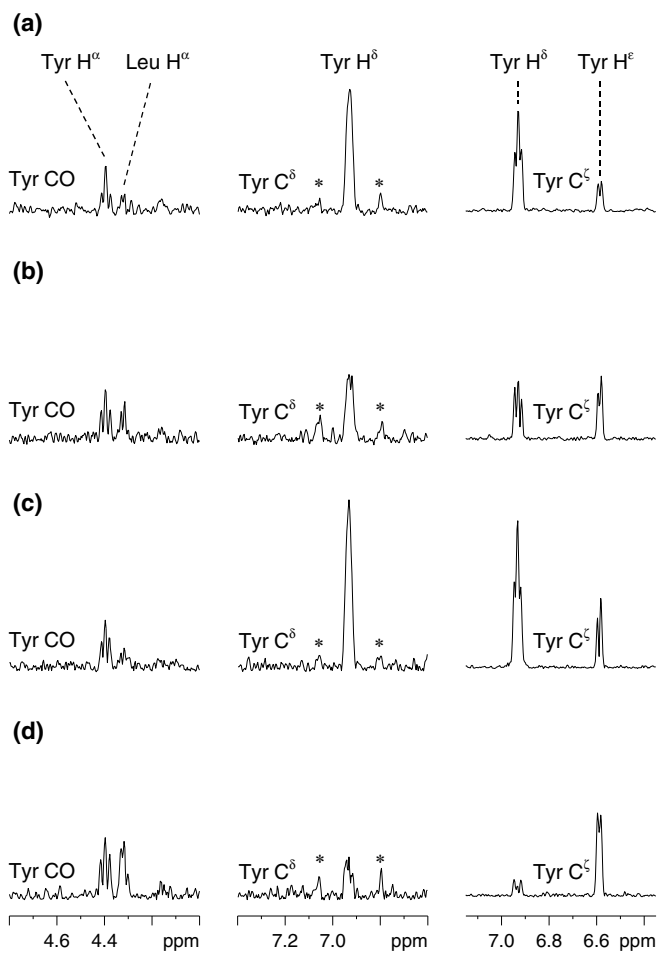

FIG. 8. The 1D sections as indicated in Fig. 7 from (a) MBOB long-range correlation spectrum $\Delta = 80.0$, 67.4, 65.2, and 63.7 ms (see Table 4, row 4); (b) *ultra*-MBOB long-range correlation spectrum, same parameters and processing as (a) except $\Delta = 106.6$, 101.6, 81.5, and 77.6 ms (Table 4, row 1); (c) HMBC spectrum recorded with the same parameters as (a) except $\Delta = 65$ ms and 256 scans to achieve equal numbers of scans for each FID in the resulting data set; (d) HMBC spectrum recorded with the same parameters as (c) except $\Delta =$ 100 ms (compare Table 4, rows 15 and 16, respectively). Minute residual signals due to ^1J couplings are marked by asterisks ($*$).

CONCLUSIONS

We have derived parameter sets for problem-adapted long-range correlation experiments MBOB, broadband HMBC, and broadband XLOC. The MBOB techniques allow for

simultaneously observing the long-range and the one-bond correlations. Depending on the window of interest in the long-range domain, the experimental parameters can be chosen from the tables provided. As demonstrated both theoretically and experimentally, the new experiments are more sensitive than conventional ones, and in particular, gaps of zero transfer amplitude are avoided throughout the range of interest. This is of particular advantage when recording spectra of unknown substances. Moreover, specially tailored *ultra*-experiments (MBOB, HMBC, XLOC) are parameterized in order to observe small long-range coupling constants far below the Lorentzian linewidth while maintaining nonvanishing cross peaks for the larger J's.

EXPERIMENTAL

Tetracycline hydrochloride was purchased from Sigma–Aldrich Co. The tetrapeptide Ac-Gln-Tyr-Leu-Gly-HMBA-Gly-Gly was synthesized on SPOCC-1500 resin (*14*) using standard solid-phase peptide synthesis protocols (*15, 16*). Fmoc-Gly-Gly and Fmoc-Gly were esterified onto the resin and the 4-Hydroxymethylbenzoic acid (HMBA) linker, respectively, using the condensing agent 1-(2-mesitylenesulfonyl)-3-nitro-1H-1,2,4-triazole (MSNT) in combination with *N*-methylimidazole as catalyst. The loading of the resin was 0.42 mmol/g. HMBA assembly and peptide elongation was achieved with TBTU-activated HMBA/Fmoc-amino acid derivatives. Final acetylation was accomplished with 10% acetic anhydride in the presence of *N*-Ethyldiisopropylamine. The target peptide was confirmed by ^{1}H and ^{13}C HR-MAS NMR on resin and by ESI-MS following cleavage under basic conditions calc: [M (Ac-Gln-Tyr-Leu-Gly-OH)] = 521.56 Da; found (MH^{+}), m/z 522.56.

The NMR spectra were recorded on a Bruker DRX 600 in standard configuration using an inverse 5-mm triple-resonance TXI probe equipped with a three-axis gradient system for liquid phase spectra. HR-MAS spectra of swollen resin were obtained with an inverse 4-mm double-resonance (^{1}H/^{13}C) HR-MAS probe equipped with a magic-angle gradient system. The gradient duration was adjusted to be a multiple of 6 over the spinning speed of 4800 Hz. Gradient pairs for coherence pathway selection were separated by a delay of a multiple of 2 over the spinning speed. ZrO_2 rotors with PTFE spacer containing a sample volume of 50 μl were utilized. XWINNMR 2.6 was used for processing and linear prediction; MBOB data editing and combination was performed with the MBOB software package (*8*).

ACKNOWLEDGMENTS

T.S.H. thanks *Deutsche Forschungsgemeinschaft*, DFG, for the research grant SCHU-1374/1-1. Support by the Danish National Research Foundation is gratefully acknowledged.

REFERENCES

1. A. Bax and M. F. Summers, *J. Am. Chem. Soc.* **108,** 2093–2094 (1986).
2. A. Meissner and O. W. Sørensen, *Magn. Reson. Chem.* **38,** 981–984 (2000).
3. M. D. Sørensen, S. M. Kristensen, J. J. Led, and O. W. Sørensen, *J. Magn. Reson. A* **103,** 364–368 (1993).
4. M. D. Sørensen, J. J. Led, and O. W. Sørensen, *J. Biomol. NMR* **4,** 135–141 (1994).
5. H. Thøgersen and O. W. Sørensen, *J. Magn. Reson. A* **110,** 118–120 (1994).
6. A. Meissner and O. W. Sørensen, *Magn. Reson. Chem.* **39,** 49–52 (2001).
7. A. Bax, K. Farley, and G. S. Walker, *J. Magn. Reson. A* **119,** 134–138 (1996).
8. MBOB software (for Bruker and Varian spectrometers) operating in full automation, i.e., performing the experiment and plotting the edited long-range and one-bond spectra, is available via http://www.crc.dk/nmr/.
9. N. C. Nielsen, H. Bildsøe, H. J. Jakobsen, and O. W. Sørensen, *J. Magn. Reson.* **66,** 456–469 (1986).
10. O. W. Sørensen, S. Dønstrup, H. Bildsøe, and H. J. Jakobsen, *J. Magn. Reson.* **55,** 347–354 (1983).
11. E. Breitmeier and W. Voelter, "Carbon-13 NMR Spectroscopy," 3rd ed., p. 140, VCH, Weinheim (1987).
12. J. A. Nelder and R. Mead, *Comp. J. (UK)* **7,** 308–313 (1965).
13. MATLAB is a matrix manipulation package, see "MATLAB Reference Guide," The Math Works Inc., Natick, MA (1999).
14. J. Rademann, M. Grøtli, M. Meldal, and K. Bock, *J. Am. Chem. Soc.* **121,** 5459–5466 (1999).
15. B. Blankemeyer-Menge, M. Nimitz, and R. Frank, *Tetrahedron Lett.* **31,** 1701–1704 (1990).
16. R. Knorr, A. Trzeciak, W. Bannwarth, and D. Gillessen, *Tetrahedron Lett.* **30,** 1927–1930 (1989).